

Estimating threshold-exceeding probability maps of environmental variables with Markov chain random fields

Weidong Li · Chuanrong Zhang · Dipak K. Dey · Shanqin Wang

Published online: 14 April 2010
© Springer-Verlag 2010

Abstract Estimating and mapping spatial uncertainty of environmental variables is crucial for environmental evaluation and decision making. For a continuous spatial variable, estimation of spatial uncertainty may be conducted in the form of estimating the probability of (not) exceeding a threshold value. In this paper, we introduced a Markov chain geostatistical approach for estimating threshold-exceeding probabilities. The differences of this approach compared to the conventional indicator approach lie with its nonlinear estimators—Markov chain random field models and its incorporation of interclass dependencies through transiograms. We estimated threshold-exceeding probability maps of clay layer thickness through simulation (i.e., using a number of realizations simulated by Markov chain sequential simulation) and interpolation (i.e., direct conditional probability estimation using only the indicator values of sample data), respectively. To evaluate the approach, we also estimated those probability maps using sequential indicator simulation and indicator kriging interpolation. Our results show that (i) the Markov chain approach provides an effective alternative for spatial uncertainty assessment of environmental spatial variables and the probability maps from this approach are more

reasonable than those from conventional indicator geostatistics, and (ii) the probability maps estimated through sequential simulation are more realistic than those through interpolation because the latter display some uneven transitions caused by spatial structures of the sample data.

Keywords Environmental evaluation · Geostatistics · Spatial uncertainty · Transiogram

1 Introduction

In environmental modeling, estimating the probability of an environmental spatial variable (not) exceeding a threshold (or cutoff) value is an effective method for spatial (i.e., locational) uncertainty assessment, which is crucial for environmental evaluation and decision making (Goovaerts 1997; Chiles and Delfiner 1999; Gaus et al. 2003; Arbia et al. 2007). For example, some threshold values of soil attributes, such as soil lead content, soil water content or soil clay content, may be critical standards for judging the quality (e.g., severely polluted, moderately polluted, or not polluted) or identifying the cropping suitability of the land under study (Goovaerts et al. 1997; Goovaerts 2001). Thus, the probability map of an important attribute (not) exceeding a threshold value will provide crucial quantitative information to policy makers for deciding remediation measures and to researchers for effectively studying related phenomena and processes (van Meirvenne and Goovaerts 2001; Lark and Ferguson 2004; Schnabel et al. 2004; Yang et al. 2008). In addition, estimating a series of threshold-exceeding probabilities is also the way used to construct the cumulative conditional probability distribution of a continuous spatial variable at an unsampled location for simulating the continuous

W. Li (✉) · S. Wang
College of Resources and Environment, Huazhong Agricultural University, Wuhan 430070, China
e-mail: weidong6616@yahoo.com

W. Li · C. Zhang
Department of Geography and Center for Environmental Sciences and Engineering, University of Connecticut, Storrs, CT 06269, USA

D. K. Dey
Department of Statistics, University of Connecticut, Storrs, CT 06269, USA

variable using Sequential Indicator Simulation (SIS) (Journel and Isaaks 1984; Deutsch and Journel 1998; Goovaerts 1999; Wang et al. 2002; Jager et al. 2005).

There are a variety of spatial statistical approaches which may be used for estimating threshold-exceeding probabilities, such as indicator kriging (Journel 1983), disjunctive kriging (Armstrong and Matheron 1986), generalized linear model (Gotway and Stroup 1997), and clipped Gaussian random fields (de Oliveira 2000). Among these approaches, indicator kriging has been more frequently used in applications in environmental sciences due to its computational efficiency and well implementation in software. Application studies may be found in Goovaerts et al. (1997), van Groenigen et al. (1997), Atkinson (1999), Brus et al. (2002), Juang et al. (2004), Lark and Ferguson (2004), and others. But it is also known that this approach has some caveats, such as no guarantee that estimated probabilities lie in $[0, 1]$. It was argued that “most indicator kriging applications rely on a flawed probabilistic model”. The effects of using such flawed model on inference about the binary map are unclear (de Oliveira 2000). For estimating the probability of a continuous spatial variable Z not exceeding a threshold value k , the common way is to define an indicator (or binary) variable on the threshold as a function of the variable under study, with one indicator value being 1 for $Z \leq k$ and the other being 0 for $Z > k$.

Indicator kriging was initially proposed by Switzer (1977) for estimation of the distribution function of a stationary random field, and later extended by Journel (1983) as a non-parametric method for prediction in random fields and used by Solow (1986) for prediction in binary random fields (de Oliveira 2000). This approach was well explored and implemented in geostatistics (Deutsch and Journel 1998). In Goovaerts (1997), two indicator kriging based methods (or strategies) were introduced for estimating threshold-exceeding probabilities: one is to estimate the probability directly from sample data using indicator kriging (IK)—an IK-based *interpolation* method; the other is to estimate the probability from a set of simulated realizations generated by SIS—a SIS-based stochastic *simulation* method. Note that SIS is a sequential simulation algorithm based on IK (i.e., it uses IK models as its estimators). Although we found no literature in studying their differences in estimated results, the latter method was usually thought to be more reasonable, as simulated realizations by sequential simulation algorithms are generally regarded as a representation of joint uncertainty about the attribute's values at multiple locations or in an area. For example, recently Juang et al. (2004) used SIS to assess the spatial uncertainty of heavy metal Cu concentration in soils, and Zhao et al. (2005) used the same method to assess the spatial uncertainty in soil organic carbon density mapping.

Recently, Markov chain geostatistics (MCG) (Li 2007a) was proposed as a new idea for simulating categorical spatial variables, such as soil types, layers and textural classes. Although it is only preliminarily developed, this approach has demonstrated some apparent advantages (e.g., higher accuracy) over SIS in simulation of soil types (Li and Zhang 2007). Except for using nonlinear estimators, the major differences of the MCG approach compared to conventional indicator kriging geostatistics include: (i) incorporating various interclass relationships (e.g., cross-correlations, juxtapositions, asymmetric sequences) through a transition probability-based asymmetric spatial correlation measure—transiogram; (ii) avoiding the well-known shortcomings encountered in conventional indicator kriging geostatistics (e.g., estimated probabilities may show order relation violation, not sum to 1 or be outside the interval $[0, 1]$) (Deutsch and Journel 1998, pp. 81–86); and (iii) generating polygon-like patterns in simulated realizations. In addition, Markov chain random field (MCRF) models—the estimators of MCG—make use of the conditional independence of nearest known neighbors in cardinal directions, rather than calculate a set of optimal weights as did in kriging. Although MCRF models always need to use both auto and cross transiograms, the inference of transiogram models is not difficult because it does not require a linear model of coregionalization (Li 2007b; Zhang and Li 2008a).

As a geostatistical approach proposed for simulating categorical variables, MCG may also be used in the same way as conventional indicator geostatistics for estimating threshold-exceeding probabilities. In this paper, we introduce how to use MCG to estimate threshold-exceeding probability maps of a continuous environmental spatial variable and conduct a case study on estimating the threshold-exceeding probability maps of clay layer thickness in alluvial soils in a region to demonstrate the features of this new approach. The objectives are: (1) to test the feasibility of using MCG to estimate threshold-exceeding probabilities, (2) to provide a new alternative in geostatistics for environmental risk assessment, and (3) to explore the differences in estimated probabilities by MCG and indicator kriging using the aforementioned two methods based on interpolation and sequential simulation.

2 Methodology

2.1 Data coding

A threshold value splits the values of a continuous spatial variable Z into two classes, that is, values not greater than the threshold and values greater than it. In MCRF models, these two classes can be labeled as symbols (or called

indicators) 1 and 2 (or A and B), respectively; that is, given a threshold value z_r , data $z(\mathbf{u}_z)$ are coded according to the following rule:

$$i(\mathbf{u}_z; z_r) = \begin{cases} 1 & \text{if } z(\mathbf{u}_z) \leq z_r \\ 2 & \text{otherwise} \end{cases}, \tag{1}$$

where $z(\mathbf{u}_z)$ represents a realization of the random variable Z at an informed location \mathbf{u}_z . Since both classes are used in modeling, we may call them class 1 and class 2 (or indicator 1 and indicator 2), respectively. Therefore, for a threshold value, we obtain a sample indicator data set of a binary variable; and for the binary variable we use four (two auto and two cross) transiograms to describe the correlations within and between the two threshold classes.

Note that we use 1 and 2 as indicators in MCG, rather than use 0 and 1 as used in conventional indicator geo-statistics. The reason is that indicators in MCG are just used as labels to denote different classes, not used as probability values in calculation. MCRF equations do not involve any indicator values. On the contrary, in indicator kriging equations, indicators (0 and 1) are directly used as probability values in calculation.

2.2 Transiogram modeling

A transiogram $p_{ij}(\mathbf{h})$ refers to a function of a transition probability from class i to class j over the distance lag \mathbf{h} . An auto-transiogram $p_{ii}(\mathbf{h})$ represents the self-dependence (i.e., auto-correlation) of a single class i and a cross-transiogram $p_{ij}(\mathbf{h})(i \neq j)$ represents the cross-dependence of class j on class i . For convenience of use, class i is called a head class and class j is called a tail class in a transiogram $p_{ij}(\mathbf{h})$. An experimental transiogram can be directly calculated from sample data by counting transition frequencies from a class to itself or another class with different distance lags by using the following equation:

$$\hat{p}_{ij}(\mathbf{h}) = F_{ij}(\mathbf{h})/N_i(\mathbf{h}) \tag{2}$$

where $N_i(\mathbf{h}) = \sum_{j=1}^n F_{ij}(\mathbf{h})$ is the total of elements in the i th row in a transition frequency matrix at the lag \mathbf{h} , $F_{ij}(\mathbf{h})$ represents the frequency of transitions from class i to class j at the lag \mathbf{h} , and n is the total number of classes (Li 2007b). To acquire reliable experimental transiograms from sparse samples one usually has to consider to use a lag tolerance $\Delta\mathbf{h}$ around each specific lag value, which may be decided by users according to the sample density. One may estimate experimental transiograms omni-directionally. But to account for anisotropies, one has to consider an appropriate tolerance angle.

Transiograms have some special properties related to transition probabilities and transition probability matrix, which can be used in transiogram modeling as constraint

conditions and also simplify the transiogram modeling burden. Some relevant properties are listed as follows: (1) transiograms are always non-negative; (2) transiograms with a common head class sum to one at any lag value; (3) transiograms are normally asymmetric, but if they are estimated bi-directionally or omni-directionally they follow the *detailed balance* condition as mentioned later; (4) the theoretical sill of a transiogram is equal to the proportion of the tail class (Li 2007b). Based on these properties, experimental transiograms for mutually exclusive classes are easy to model because expert knowledge can be readily used in the modeling process (Li and Zhang 2007).

One way to acquire transiogram models for Markov chain modeling is to use appropriate mathematical models to fit experimental transiograms (Li 2007b). The model fitting needs to be conducted subset by subset jointly so as to meet the summing-to-one condition

$$\sum_{j=1}^n p_{ij}(\mathbf{h}) = 1, \tag{3}$$

where n is the number of classes. Note that here a subset refers to all of the transiograms with the same head class i . To ensure the condition (3), one of transiogram models $p_{ik}(\mathbf{h})$ in the subset may take the left part of unity minus the sum of all other transiogram models as

$$p_{ik}(\mathbf{h}) = 1 - \sum_{\substack{j=1 \\ j \neq k}}^n p_{ij}(\mathbf{h}). \tag{4}$$

Thus, that experimental transiogram $\hat{p}_{ik}(\mathbf{h})$ does not need to be fitted with a mathematical model.

The quantitative relationship between cross-transiograms $p_{ij}(\mathbf{h})$ and $p_{ji}(\mathbf{h})$ can also be used in transiogram modeling. If transiograms are estimated bi-directionally or omni-directionally rather than uni-directionally (e.g., from North to South), cross-transiograms obey the following relationship (called the detailed balance condition)

$$p_{ij}(\mathbf{h}) = \frac{p_j}{p_i} \cdot p_{ji}(\mathbf{h}), \tag{5}$$

where p_i and p_j are proportions of class i and class j , respectively. Thus, if the transiogram model $p_{ji}(\mathbf{h})$ and the class proportions p_i and p_j are known, the transiogram model $p_{ij}(\mathbf{h})$ can be directly obtained using Eq. 5.

To estimate the probability of (not) exceeding a threshold value, we need to consider both the spatial auto-correlations of the two threshold classes (i.e., class 1 and class 2) and their cross-correlations. Thus, four transiogram models, i.e., $p_{11}(\mathbf{h})$, $p_{12}(\mathbf{h})$, $p_{21}(\mathbf{h})$ and $p_{22}(\mathbf{h})$ are needed. Assume we have obtained the transiogram model $p_{11}(\mathbf{h})$ from the experimental transiogram $\hat{p}_{11}(\mathbf{h})$. Using the above relationships (4) and (5), we can directly calculate the other three transiogram models as follows:

$$p_{12}(\mathbf{h}) = 1 - \sum_{\substack{j=1 \\ j \neq 2}}^2 p_{1j}(\mathbf{h}) = 1 - p_{11}(\mathbf{h}) \quad (6)$$

$$p_{21}(\mathbf{h}) = \frac{p_1}{p_2} \cdot p_{12}(\mathbf{h}) = \frac{p_1}{p_2} \cdot [1 - p_{11}(\mathbf{h})] \quad (7)$$

$$p_{22}(\mathbf{h}) = 1 - p_{21}(\mathbf{h}) = 1 - \frac{p_1}{p_2} \cdot [1 - p_{11}(\mathbf{h})]. \quad (8)$$

Thus, as long as we acquire one transiogram model among the four needed transiogram models, the other three can be simply inferred according to the above relationships (6–8). Because we normally do not need to use unidirectional transiograms in horizontal two-dimensional Markov chain modeling, the above relationships are widely applicable. Hence, to model a threshold-exceeding probability using the MCG approach, the workload of transiogram modeling is no more than modeling a single indicator auto-variogram. In addition, because the sill of a transiogram model can be simply set to the proportion of the corresponding tail class, it is actually easier to model an experimental transiogram than to model an experimental indicator variogram. The above quantitative relationships (6–8) also imply that for a threshold value the four related transiograms theoretically should have equal correlation ranges.

A mathematical model can fit only the general trend of an experimental transiogram. However, experimental transiograms sometimes may exhibit complex shapes. When sufficient sample data are available to provide reliable experimental transiograms (here “reliable” means the shape of an experimental transiogram becomes stable with increasing number of samples), the complex shape of a reliable experimental transiogram should be regarded as the real reflection of the heterogeneity of the variable under study. Under this situation it is preferable to capture the complex shape of the experimental transiogram in transiogram modeling. An easy and effective way to acquire transiogram models with the features of experimental transiograms is to simply interpolate discrete experimental transiograms into continuous models. There may be various methods for conducting the interpolation. The linear interpolation method for such a purpose is

$$p_{ij}(\mathbf{h}) = \frac{\hat{p}_{ij}(\mathbf{h}_k) \cdot (\mathbf{h}_{k+1} - \mathbf{h}) + \hat{p}_{ij}(\mathbf{h}_{k+1}) \cdot (\mathbf{h} - \mathbf{h}_k)}{\mathbf{h}_{k+1} - \mathbf{h}_k}, \quad (9)$$

where \mathbf{h}_{k+1} and \mathbf{h}_k are the corresponding lags of two estimated neighboring values in an experimental transiogram, and $p_{ij}(\mathbf{h})$ is the value to be interpolated (or estimated) at the lag \mathbf{h} between \mathbf{h}_{k+1} and \mathbf{h}_k (Li and Zhang 2007). The mathematical validity of the above Eq. 9 was proved in Li and Zhang (2009). Here to deal with binary variables, we also can get one transiogram model through interpolation using Eq. 9 and then infer the other three using the above Eqs. 6–8.

2.3 Markov chain random field models

MCRF models are needed for estimating local conditional probabilities of occurrence of classes at uninformed locations from several nearest known neighbors (sampled or previously estimated locations). Similar to the transiogram idea, the MCRF idea was proposed also as a consequence of a long-time effort to correct the deficiencies of earlier multidimensional Markov chain models such as underestimation of small classes, shortage of generalization, and difficulty of conditioning to sample data (Li 2007a; Zhang and Li 2008b). Assume Z is a random variable, which obeys the properties of MCRFs, defined on a state space $S = (1, 2, \dots, n)$, and $z(\mathbf{u})$ represents a specific realization of Z at the location \mathbf{u} . If we consider only one nearest known data location in each of the four cardinal directions, the general MCRF model is given as (Li 2007a)

$$\begin{aligned} \Pr[z(\mathbf{u}) = k | (N)] &= \Pr[z(\mathbf{u}) = k | z(\mathbf{u}_1)] \\ &= l_1, z(\mathbf{u}_2) = l_2, z(\mathbf{u}_3) = l_3, z(\mathbf{u}_4) = l_4 \\ &= \frac{p_{l_1 k}(\mathbf{h}_1) \prod_{g=2}^4 p_{kl_g}(\mathbf{h}_g)}{\sum_{f=1}^n \left[p_{l_1 f}(\mathbf{h}_1) \prod_{g=2}^4 p_{fl_g}(\mathbf{h}_g) \right]} \end{aligned} \quad (10)$$

where, (N) refers to all of the data in different directions (i.e., samples for interpolation, or samples plus previously simulated data for sequential simulation); $\mathbf{h}_1, \mathbf{h}_2, \mathbf{h}_3$, and \mathbf{h}_4 represent the distances from the location \mathbf{u} being estimated to its nearest known neighbors $\mathbf{u}_1, \mathbf{u}_2, \mathbf{u}_3$, and \mathbf{u}_4 in four cardinal directions, respectively; and k, f and l_g ($g = 1, \dots, 4$) represent the states of the Markov chain (or the random variable Z) at the five locations $\mathbf{u}, \mathbf{u}_1, \mathbf{u}_2, \mathbf{u}_3$, and \mathbf{u}_4 , respectively, all defined on the state space S . In directions 2, 3, and 4, transitions are from the current location \mathbf{u} to its nearest known neighbors, but in direction 1 (i.e., the coming direction of the Markov chain), the transition is from the nearest known neighbor \mathbf{u}_1 to the current location \mathbf{u} . The above general model is illustrated in Fig. 1a.

The above solution is used for modeling categorical variables. To model the probabilities of a continuous attribute (not) exceeding a threshold value z_r , we need to consider two threshold classes: 1 for $z(\mathbf{u}) \leq z_r$ and 2 for $z(\mathbf{u}) > z_r$. Thus, the above equation can be rewritten as

$$\begin{aligned} F[\mathbf{u}; z_r | (N)] &= \Pr[z(\mathbf{u}) \leq z_r | (N)] = \Pr[z(\mathbf{u}) = 1 | z(\mathbf{u}_1)] \\ &= l_1, z(\mathbf{u}_2) = l_2, z(\mathbf{u}_3) = l_3, z(\mathbf{u}_4) = l_4 \\ &= \frac{p_{l_1 1}(\mathbf{h}_1) \prod_{g=2}^4 p_{1l_g}(\mathbf{h}_g)}{\sum_{f=1}^2 \left[p_{l_1 f}(\mathbf{h}_1) \prod_{g=2}^4 p_{fl_g}(\mathbf{h}_g) \right]} \end{aligned} \quad (11)$$

and

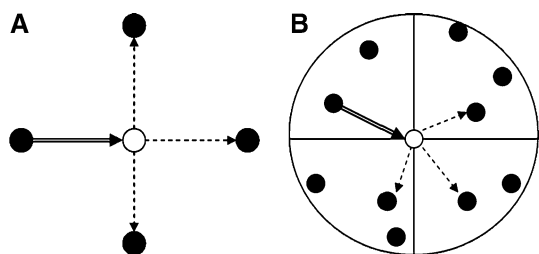


Fig. 1 Illustration of the general Markov chain random field model for four nearest known neighbors in four cardinal directions (a) and the quadrant search algorithm (b). Black cells refer to data; the white cell refers to the location to be estimated; the thick arrow represents the moving direction of the Markov chain; dash arrows represent interactions between the nearest data and the location to be estimated; and all arrows point to the directions of transition probabilities

$$\begin{aligned}
 1 - F[\mathbf{u}; z_r | (N)] &= \Pr[x(\mathbf{u}) > z_r | (N)] = \Pr[z(\mathbf{u}) = 2 | z(\mathbf{u}_1) \\
 &= l_1, z(\mathbf{u}_2) = l_2, z(\mathbf{u}_3) = l_3, z(\mathbf{u}_4) = l_4] \\
 &= \frac{p_{l_1 2}(\mathbf{h}_1) \prod_{g=2}^4 p_{2l_g}(\mathbf{h}_g)}{\sum_{f=1}^2 [p_{l_1 f}(\mathbf{h}_1) \prod_{g=2}^4 p_{fl_g}(\mathbf{h}_g)]} \quad (12)
 \end{aligned}$$

for the two classes (or indicator values) 1 and 2, respectively. It can be seen that both equations involve class 1 and class 2 because f and l_g ($g = 1, \dots, 4$) all represent states defined on the state space $S = (1, 2)$.

For a specific unobserved location to be estimated, a further simplified form of the model (10) may be needed because the numbers of the nearest known neighbors found in a search circle, one per quadrant, may be fewer than four at some places. This is especially true for locations close to edges. For internal locations, if samples are too sparse and the search radius is small, at the beginning stage of a simulation the nearest known neighbors found within quadrants of a search circle may also be less than four. Thus situations with less than four nearest known neighbors must also be considered. Under the situations of having three, two and one nearest known neighbor(s), for class 1 Eq. 11 can be simplified as

$$\begin{aligned}
 \Pr[z(\mathbf{u}) \leq z_r | (N)] &= \Pr[z(\mathbf{u}) = 1 | z(\mathbf{u}_1) = l_1, z(\mathbf{u}_2) = l_2, \\
 z(\mathbf{u}_3) = l_3] &= \frac{p_{l_1 1}(\mathbf{h}_1) \prod_{g=2}^m p_{1l_g}(\mathbf{h}_g)}{\sum_{f=1}^2 [p_{l_1 f}(\mathbf{h}_1) \prod_{g=2}^m p_{fl_g}(\mathbf{h}_g)]}, \quad m = 2, 3 \quad (13)
 \end{aligned}$$

and

$$\begin{aligned}
 \Pr[z(\mathbf{u}) \leq z_r | (N)] &= \Pr[z(\mathbf{u}) = 1 | z(\mathbf{u}_1) = l_1] \\
 &= \frac{p_{l_1 1}(\mathbf{h}_1)}{\sum_{f=1}^2 [p_{l_1 f}(\mathbf{h}_1)]} = p_{l_1 1}(\mathbf{h}_1), \quad (14)
 \end{aligned}$$

respectively. Note that as long as one nearest known neighbor can be found, that location should serve as the location \mathbf{u}_1 —the location from which the Markov chain

comes. In case that no one nearest known neighbor can be found within a search circle, we have

$$\Pr[z(\mathbf{u}) \leq z_r | (N)] = \Pr[z(\mathbf{u}) = 1] = p_1, \quad (15)$$

where p_1 is the proportion of class 1, which equals the theoretical sill of transiograms $\hat{p}_{11}(\mathbf{h})$. Equation 15 is based on the following rational assumption: The Markov chain comes from a location outside the search circle, far away from the current location being estimated. Because its last stay location is beyond the correlation range, its influence to the current location can be ignored. After moving sufficient distance (or spatial steps) the Markov chain reaches its current location with a stable probability distribution—its class proportions, which is a basic property of Markov chains.

Equation 12 can be simplified similarly for class 2.

2.4 Search algorithm

In practice, to deal with irregular data in the whole space, the cardinal directions have to cover the whole area of a search circle so that no nearest known neighbor will be missed. This requires the cardinal directions be replaced by the equally split search sectors of the search circle such as quadrants. Such a replacement is necessary and also acceptable to MCRF models because the requirement of cardinal directions in the conditional independence assumption of nearest known neighbors is not very strict in applications. The quadrant search algorithm is shown in Fig. 1b. When estimating the conditional probability distribution of an attribute at an uninformed location, the algorithm will look for one nearest known neighbor from each quadrant (if there are known neighbors in the quadrant). The nearest known neighbors finally found from all quadrants constitute the MCRF model for estimating the attribute at the uninformed location. The quadrant search is not a new idea; as it is explained in the Websters-online-dictionary, quadrant search is “similar to octant search, but using four sectors instead of eight sectors. (It) applies to any interpolation method where a limited number of sample datapoints are used to estimate intermediate values” (Staff of the U.S. Bureau of Mines 1996). As to how to choose the search radius, it is users’ decision based on the density of their samples. However, one principle is that it should avoid using such a small search radius that the search circle frequently covers no or less than four nearest known neighbors. Testing in simulation of soil types showed that the MCRF sequential simulation (MCSS) algorithm which employed quadrant search was not only applicable but also demonstrated obvious advantages over conventionally used sequential indicator simulation (Li and Zhang 2007).

With the MCRF models serving as the estimator and the above search algorithm, MCG can estimate the threshold-exceeding probabilities at uninformed locations directly from samples (i.e., MCRF-based interpolation method) or estimate them from a number of simulated realizations generated by the MCSS algorithm (i.e., MCSS-based simulation method).

2.5 Indicator kriging

Threshold-exceeding probabilities can be estimated directly by IK or indirectly through a number of simulated realizations by SIS—an IK-based sequential simulation algorithm (Goovaerts 1997; Deutsch and Journel 1998). In IK, a continuous variable is coded as indicator values 1 and 0 at a threshold. Given a threshold value z_r , sample data $z(\mathbf{u}_\alpha)$ are coded according to the following rule:

$$i(\mathbf{u}_\alpha; z_r) = \begin{cases} 1 & \text{if } z(\mathbf{u}_\alpha) \leq z_r \\ 0 & \text{otherwise} \end{cases} \tag{16}$$

Using ordinary IK as an example, the probability of the continuous random variable Z not exceeding the threshold value z_r at an uninformed location \mathbf{u} is estimated by the following rule:

$$[F(\mathbf{u}; z_r | (N))]^* = [\Pr(z(\mathbf{u}) \leq z_r | (N))]^* = \sum_{\alpha=1}^{N(\mathbf{u})} \lambda_\alpha(\mathbf{u}; z_r) i(\mathbf{u}_\alpha; z_r), \tag{17}$$

where (N) represents the number of data in the neighborhood of location \mathbf{u} , and $\lambda_\alpha(\mathbf{u}; z_r)$ is the weight assigned to the indicator value $i(\mathbf{u}_\alpha; z_r)$ at location \mathbf{u}_α . The weight $\lambda_\alpha(\mathbf{u}; z_r)$ is given by an ordinary kriging system

$$\begin{cases} \sum_{\beta=1}^{N(\mathbf{u})} \lambda_\beta(\mathbf{u}; z_r) C(\mathbf{u}_\alpha - \mathbf{u}_\beta; z_r) + \mu(\mathbf{u}; z_r) \\ = C(\mathbf{u}_\alpha - \mathbf{u}; z_r), \alpha = 1, \dots, N(\mathbf{u}), \\ \sum_{\beta=1}^{N(\mathbf{u})} \lambda_\beta(\mathbf{u}; z_r) = 1 \end{cases} \tag{18}$$

where C represents the indicator covariance between any two data in the neighborhood of location \mathbf{u} (Goovaerts 1997 pp. 293–294).

Equation 17 clearly shows that when estimating the threshold-exceeding probability at an uninformed location the 0 indicator values within the neighborhood do not make contribution. Thus, if all of the data in the kriging neighborhood have an indicator value 0, the threshold-exceeding probability at the uninformed location must be zero.

In IK, the search algorithm does not consider cardinal directions because correlations between data are also incorporated in estimation of data weights, and the neighborhood may consider more than four data. In addition,

indicator kriging uses only one indicator auto variogram for estimating threshold-exceeding probabilities.

2.6 Sequential simulation and interpolation

For each approach (conventional indicator geostatistics or Markov chain geostatistics), sequential simulation and interpolation actually use the same estimator (i.e., models for estimating local conditional probabilities. For MCG they are Eqs. 11–16). Their differences lie with conditioning data, visiting path and whether or not using Monte Carlo simulation. The IK-based interpolation method for threshold-exceeding probability estimation includes the following steps:

- Step 1: Discretize the study area into a grid of pixels and insert the sample indicator data (1 and 0) into the grid.
- Step 2: Choose a proper search radius.
- Step 3: Visit each unsampled pixel of the grid only once along a path (usually row by row from left to right).
- Step 4: At each unsampled pixel, estimate the probability of not exceeding the threshold value using an IK model and sample indicator data within the search circle centered on the unsampled pixel.

The MCRF-based interpolation method is similar except that (i) it uses a MCRF model, (ii) it uses only four nearest data, one per quadrant, within the search circle, or less if no data found in some quadrants, and (iii) it uses 1 and 2 as indicators.

The SIS-based simulation method for threshold-exceeding probability estimation includes the following steps:

- Step 1: Discretize the study area into a grid of pixels and insert the sample indicator data (1 or 0) into the grid.
- Step 2: Choose a proper search radius.
- Step 3: Visit each unsampled pixel of the grid only once along a random path.
- Step 4.1: At each unsampled pixel, estimate the probability of not exceeding the threshold value using an IK model and conditioning data (including indicators of sample data and previously simulated data) within the search circle centered on the unsampled pixel.
- Step 4.2: Build a cumulative probability distribution with only two intervals using the estimated probability and its complement.
- Step 4.3: Draw a random number uniformly distributed in $[0, 1]$. The simulated indicator value at the visiting location is the one (1 or 0) that corresponds to the probability interval that include the random number.

- Step 4.4: Add the simulated value to the conditioning data set and proceed to the next unsampled pixel along the random path.
- Step 5: Repeat the procedure from Step 3 to Step 4.4 with a different random path to generate another realization.
- Step 6: Estimate the threshold-exceeding probability map from a number of realizations by counting the times of occurrence of an indicator value (1 or 0) at each pixel.

Note that here we simulated only the indicator values rather than the whole value range of the continuous variable, which is sufficient for estimating threshold-exceeding probability maps. The MCSS-based simulation method is similar to the SIS-based simulation method except that (i) it uses a MCRF model, (ii) it uses only four nearest data, one per quadrant, within the search circle, or less if no data found in some quadrants, and (iii) it uses 1 and 2 as indicators.

3 Case study

3.1 Data acquisition and analysis

Clay layers play a significant role in alluvial soils in influencing agricultural production and environmental management. For example, they may strongly affect the transport processes of field water and solute, water retention, nutrient sorption, and crop root growth in soils. In this case study we chose the clay layer thickness within 2 m soil depth at a regional scale as the studied regionalized random variable and estimated the probabilities of this variable (not) exceeding some thickness threshold values. The field sample data set was obtained in 1994. Field observations and samplings were arranged in an approximately 15 km² rectangular area around the Quzhou Experiment Station of China Agricultural University in Quzhou County, Hebei Province, China. A total of 139 observation points were arranged on a triangular grid, with a sampling interval of 350 m (except for places of villages) (Fig. 2) (Zhang and Li 2008a). The change of soil texture along each soil profile was determined by drilling boreholes and empirical hand texturing. Clay layer thickness in each soil profile was further derived from the textural layer records of profiles.

Figure 3 shows the histogram of the clay layer thickness estimated from the observed data. The histogram tends to be left-skewed. Clay layers in 2 m soil depth have an average thickness of 46.15 cm. No clay layers occur in quite a few soil profiles. Three thresholds of clay layer thickness, that is, 10, 50 and 100 cm, were chosen for

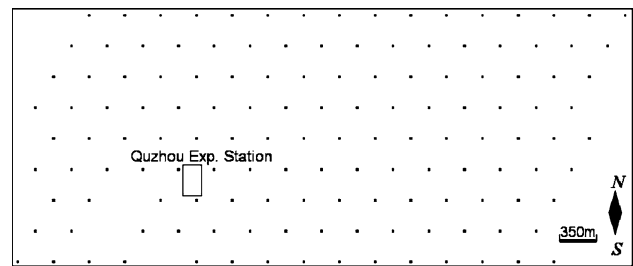


Fig. 2 Locations of observed soil profiles

probability estimation in the case study. For convenience of estimation, the study area was discretized into a 239 by 97 raster with a pixel size of 25 m by 25 m. Using the three threshold values, the 139 sample data of clay layer thickness were transformed into three indicator data sets. Omni-directional experimental transiograms were estimated from each of the indicator datasets, as shown in Figs. 4, 5 and 6. A lag tolerance of 12 pixel lengths was used in estimating experimental transiograms so as to avoid steep fluctuations.

Two sets of experimental transiograms were fitted by mathematical models: First an exponential model was used to simply fit one of them and then the other three were further calculated from the fitted model (see Figs. 4, 6). The simple model fits the first two low-lag values (except for the origin point) of the experimental transiogram well. The model fitting process follows the rules designed for modeling experimental transiograms of categorical variables (Li 2007b), that is, nugget effect is set to zero, sill is set to the proportion of the tail class, and measured low-lag values have the priority of being fitted as well as possible. In Fig. 5, the linear interpolation method of Eq. 9 is used to get transiogram models. The purpose of using these two methods is to demonstrate that both methods are applicable. These transiogram models effectively represent the spatial auto and cross correlations of the threshold classes of clay layer thickness. From Fig. 4, it can be seen that the auto-correlation range of the class 2 (i.e., $p_{22}(\mathbf{h})$, clay layer thickness > 10 cm) is about 17 pixel lengths (i.e., 425 m). The other auto and cross correlation ranges for the same threshold value can be simply inferred from the corresponding calculated transiogram models (e.g., they are the lags corresponding to 95% of sills for exponential models). It is easy to see that they are all about 425 m, as defined by the quantitative relationships in Eqs. 6, 7, and 8. Correlation ranges for other threshold values can be approximately discerned from the corresponding transiogram models as shown in Figs. 5 and 6. The correlation ranges shown on the transiograms for threshold values 50 and 100 cm are all about 450 m, which is close to that for the 10 cm threshold value.

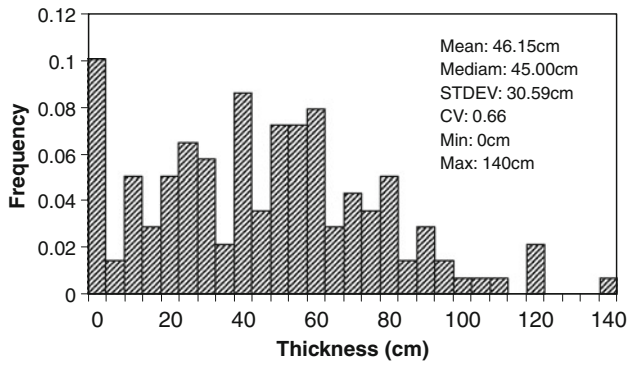


Fig. 3 Sample descriptive statistics and histogram of clay layer thickness

Omni-directional experimental indicator auto variograms were estimated from the data sets using the GSLIB software. For the thickness threshold value of 10 cm, a spherical model (range 40 pixel lengths, nugget 0.09 and sill 0.15) was used to simply fit the experimental indicator auto variogram $\hat{\gamma}_I(\mathbf{h})$. The use of a nugget effect and the free setting of the sill enable us to use a longer range to better fit all values of the experimental indicator auto-variogram. Such a model fitting follows the custom of variogram modeling in conventional geostatistics. The fitted indicator auto variogram model $\gamma_I(\mathbf{h})$ was used here for the case study.

Fig. 4 Experimental transiograms and their models of clay layer thickness for the threshold value 10 cm. Here Label 1 refers to the class of being not greater than 10 cm, and Label 2 refers to the class of being greater than 10 cm. Lags are represented using numbers of pixel length

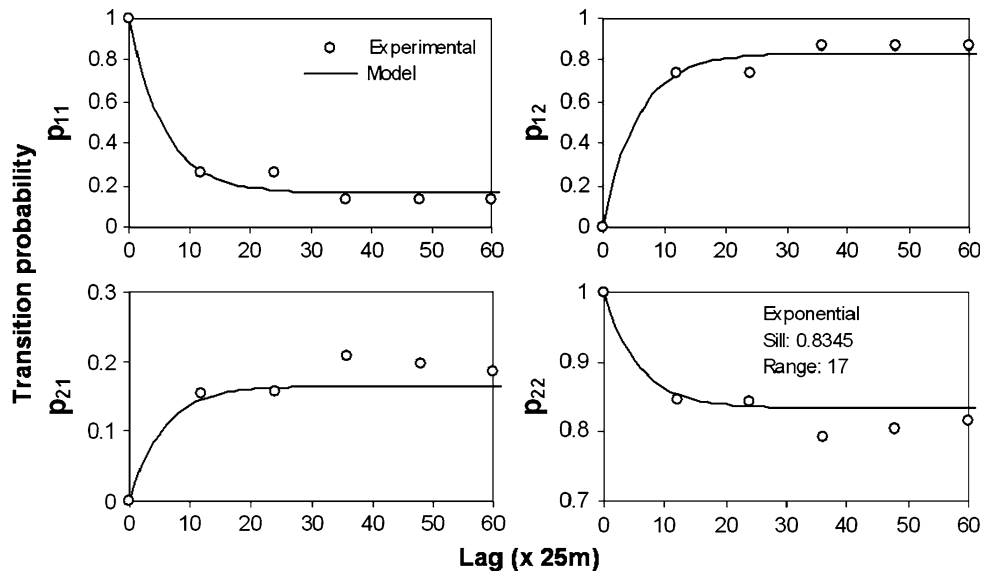


Fig. 5 Experimental transiograms and their models of clay layer thickness for the threshold value 50 cm using the linear interpolation method. Label 1 refers to the class of ≤ 50 cm and Label 2 refers to the class of >50 cm. Lags are represented using numbers of pixel length

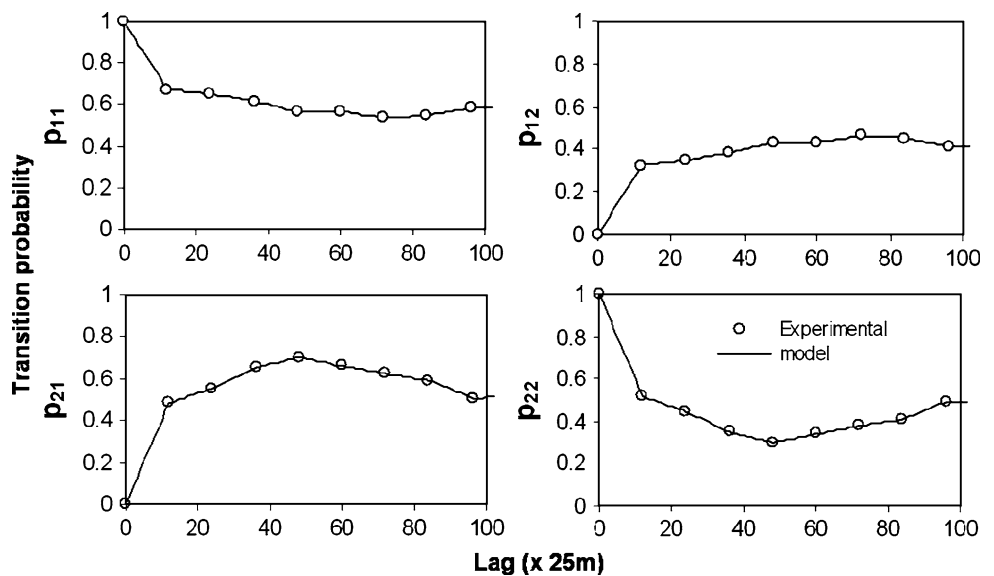
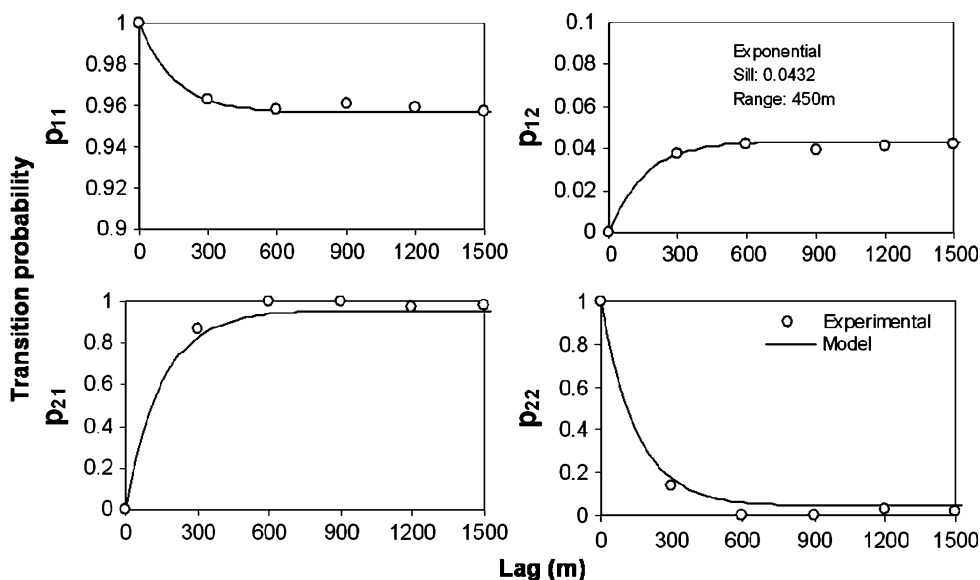


Fig. 6 Experimental transiograms and their models of clay layer thickness for the threshold value 100 cm. Label 1 refers to the class of ≤ 100 cm and Label 2 refers to the class of >100 cm. Note that here the unit of lag distance is meter



3.2 Estimated results by MCG

We first estimated the threshold-exceeding probability maps of clay layer thickness through a number of simulated realizations generated by the MCSS algorithm. Figure 7 shows those probability maps for the three thickness threshold values, each estimated from 1,000 simulated realizations. These probability maps look nice (no uneven transitions) and they clearly indicate where and with how much probability the clay layer thickness exceeds or does not exceed one of the defined thickness threshold values. These data are useful for estimating the risk of, for example, the drainage of water along soil profiles being blocked. They are also helpful for demonstrating and visualizing the uncertainty in the spatial distribution of clay layer thickness. Note that the probability maps for class 1 and class 2 of each threshold value are mutually complementary and sum to 1 at every location.

The number of simulated realizations used for probability estimation has some effects on estimated results. However, as long as the number of realizations is not very small (e.g., less than 100) the effects can be neglected. We found that the probability maps estimated from 100 realizations with different random number sequences have little difference in detail, and when the number of realizations increases to 1000 there is no visual difference for different random number sequences.

Realization maps generated here do not reflect the spatial pattern of a continuous variable because they have only two classes and do not account for the whole continuous data range of the attribute (e.g., here 0 cm to a maximum thickness value in the study area). The hardened map based on a certain probability level (e.g., 0.2, 0.5, 0.8, or 0.95) of a threshold class can, however, indicate visually the areas

where the attribute can be generally classified into some “quality grade” (e.g., good drainage condition) under the probability level (Goovaerts et al. 1997). Figure 8 shows the hardened maps of clay layer thickness being not greater than each of the three thickness threshold values at the probability levels of 0.5 and 0.25, respectively.

Besides the MCSS-based simulation method used above, we also used the MCRF-based interpolation method to estimate the probability maps of (not) exceeding each of the three thickness thresholds. Because previously estimated data in the interpolation process are not included into the conditioning data set for later estimation of other uninformed locations, whether the visiting path is random or not has no effect on interpolated results. Considering that the nearest known neighbors used in the two methods for estimating the same uninformed location are usually different (except at the beginning), the estimated results are expected to be different. Figure 9 contrasts the two probability maps of clay layer thickness being not greater than 10 cm, estimated using the two different methods respectively. It can be seen that some differences exist between them. A major difference is that the transition zones from high value areas to low value areas is very smooth in the MCSS-based probability map using the simulation method (see Fig. 9a), but not so much in the MCRF-based probability map using the interpolation method (see uneven transitions in Fig. 9b). This transition problem may be related to the spatial change of data configurations in estimation neighborhoods and the sparseness of conditioning data (only samples) in the interpolation process. On the contrary, in the simulation process the conditioning data (samples plus visited locations) quickly become abundant due to the addition of simulated data at earlier steps. The small and relatively fixed neighborhood defined

Fig. 7 Estimated probability maps of clay layer thickness (not) exceeding some thickness threshold values (i.e., 10, 50, and 100 cm)

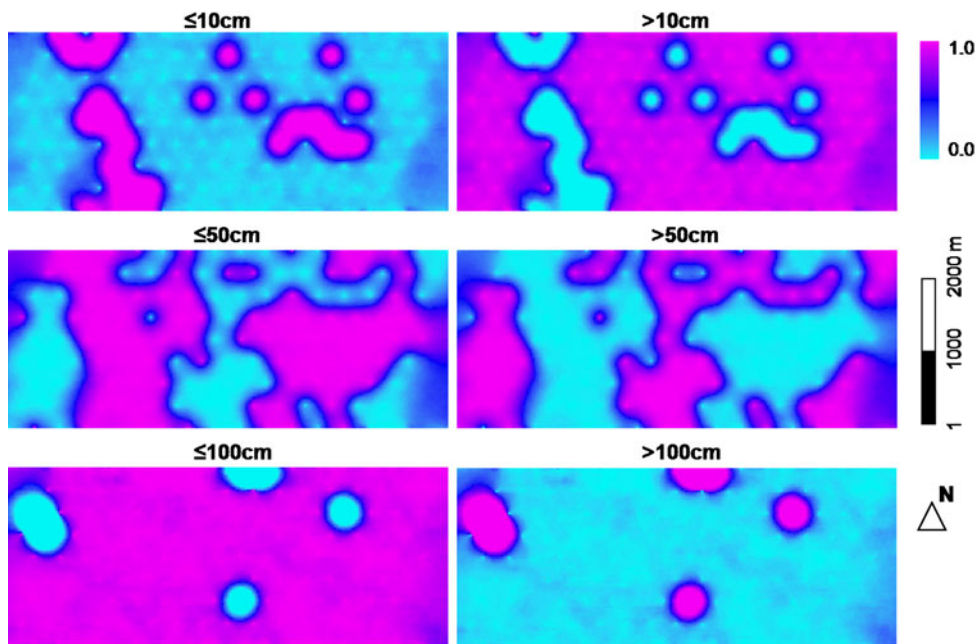
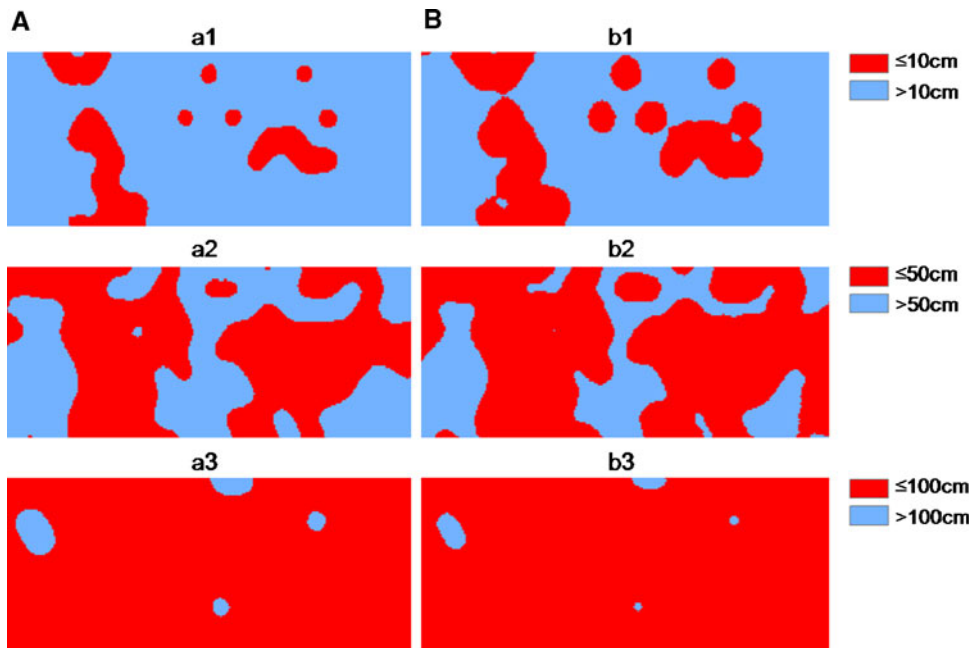


Fig. 8 Maps of clay layer thickness (not) exceeding threshold values (i.e., 10, 50, and 100 cm), hardened from estimated occurrence probabilities. **a** The red class indicates the areas where clay layer thickness is not greater than a certain threshold value at the probability level of 0.5. **b** The red class indicates the areas where clay layer thickness is not greater than a certain threshold value at the probability level of 0.25



by quadrant search and used in MCRF modeling may be the second reason for such a difference.

Obviously it is the difference between the joint estimation of probabilities at uninformed locations in sequential simulation and the separate estimation of them in interpolation that contributes to the above difference between the probability maps (i.e., the transition problem). Similar differences can also be seen from the maximum probability maps estimated using the two methods (Fig. 10). In addition, the two maximum probability maps reveal another difference: in the maximum probability map based on interpolation (see Fig. 10b), it seems each

sample point applies its influence to its vicinity isolatedly (no apparent joint effects can be seen); however, in the maximum probability map based on simulation (Fig. 10a), multiple neighboring sample points belonging to the same class, particularly those belonging to class 1, clearly generate a joint influence around them and thus form joint high probability areas. This means that by incorporating previously estimated data into the conditioning data set sequential simulation is much more reasonable for uncertainty assessment than interpolation which estimates each uninformed location purely based on the sparse samples.

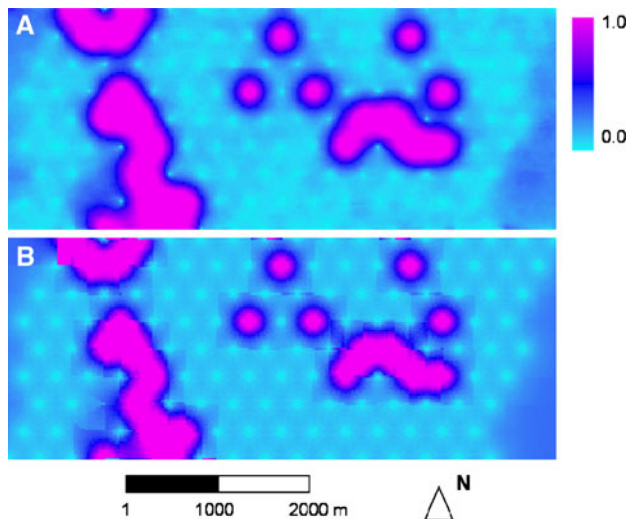


Fig. 9 Probability maps of clay layer thickness in 2 m soil depth to be ≤ 10 cm using different Markov chain random field (MCRF) estimation methods. **a** Estimated from realizations generated by MCRF sequential simulation. **b** Estimated directly from samples by MCRF interpolation

3.3 Comparison with indicator kriging

We also estimated the threshold-exceeding probability maps of clay layer thickness using conventional indicator geostatistics. Ordinary indicator kriging (oIK) was chosen as the estimator. Figure 11a, b shows the SIS-based probability map and the IK-based probability map, respectively, for clay layer thickness not exceeding the thickness threshold value 10 cm. Although both kinds of probability maps were suggested and used to represent the uncertainty of continuous variables, they actually displayed obvious differences in this case study. It can be seen that the IK-based probability map shows clear influence gradients of class 1 (i.e., ≤ 10 cm class) sample data while the SIS-based probability map does not have such features. The latter map indicates farther and also smoothly decreased influence of class 1 samples. This is because previously simulated data can pass the influence of samples to distant places when they are included into the conditioning data set for later simulation of other uninformed locations in a simulation. A common characteristic of the two probability maps is that probability values appear to be zero or close to zero at all locations beyond the influence scope of class 1 sample data, which agrees with Eq. 18. This is obviously not rational. When a class does not appear in the sparse samples in an area, it is very possible that it is just missed by the sampling; so its occurrence probability at an unsampled location in the area should not be simply zero. This irrationality of conventional indicator geostatistics is caused by the fact that indicator kriging ignores interclass correlations. In addition, without considering interclass

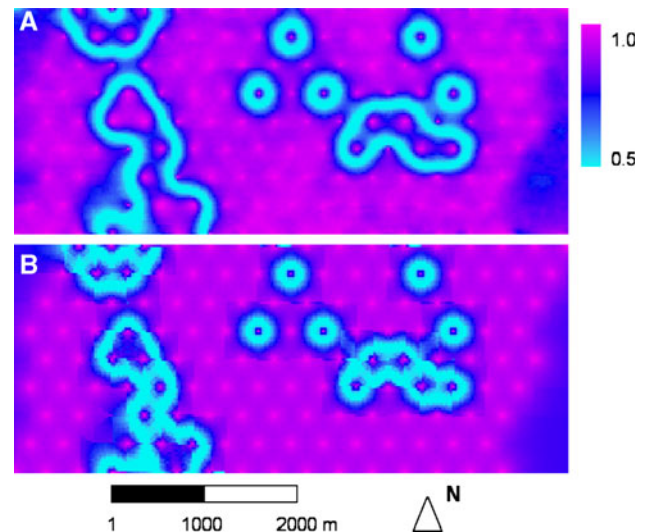


Fig. 10 Maximum probability maps of the two threshold classes of clay layer thickness in 2 m soil depth to be ≤ 10 cm using different MCRF estimation methods. **a** Estimated from realizations generated by MCRF sequential simulation. **b** Estimated directly from samples by MCRF interpolation

correlations, there is no guarantee that the estimated probability values at any unsampled location for class 1 and class 2 can sum to 1 unless one takes the complement of the other.

Three differences can be found between the MCSS-based probability map (Fig. 9a) and the SIS-based one (Fig. 11a): (a) The latter map has fuzzier or wider transition zones from the high-probability areas to zero (or low) probability areas, which should be a reflection of dispersed patterns in simulated realizations generated by SIS (Li and Zhang, 2007). (b) The SIS-based probability map has zero or close-to-zero values in the areas without class 1 (i.e., ≤ 10 cm) samples; on the contrary, the MCSS-based probability map shows obvious non-zero values in the same areas except for on exact class 2 (i.e., > 10 cm) sample locations. This means that the incorporation of cross-correlations in MCRF models has obvious contribution to the estimated probabilities. (c) In the area without samples (i.e., the right-bottom area), the SIS-based probability map has zero values but in the MCSS-based probability map the probabilities in the same area tend to equal the marginal probability of class 1 (the ≤ 10 cm class), that is, its proportion 0.1655. Apparently the latter map is more reasonable and this results from the consideration of both classes which guarantees the total probabilities sum to one. The SIS-based method considers only the contribution of a single class when estimating its occurrence probabilities. So once no data of a class are found in the neighborhood of a location, the estimated probability of the class at the location becomes zero.

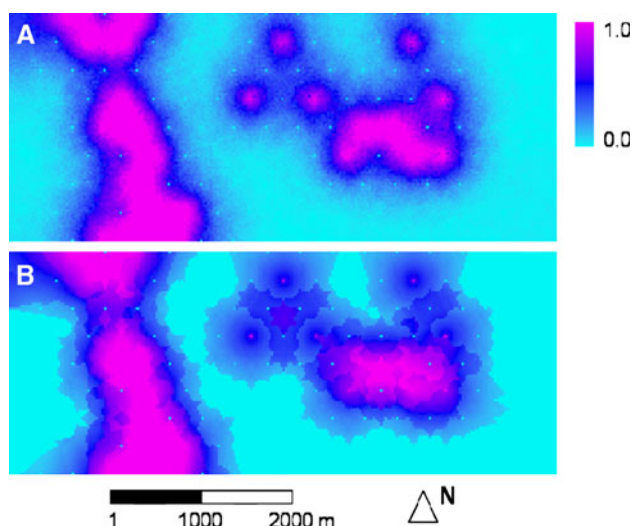


Fig. 11 Estimated probability maps of clay layer thickness being not greater than 10 cm using conventional indicator geostatistical methods. **a** Estimated from realizations generated by sequential indicator simulation. **b** Estimated directly from samples by indicator kriging interpolation

Comparing the IK-based probability map (Fig. 11b) with the MCRF-based probability map (Fig. 9b), we may find similar differences, except that the data values beyond the influence scope of class 1 samples in the IK-based map are absolutely zero and that some uneven transitions of the estimated probability values appear around class 1 sample locations in both maps. The occurrence of zero probability values of class 1 (i.e., the ≤ 10 cm class) in the areas beyond the influence scope of class 1 sample locations in the IK-based map is apparently a flaw of IK caused by ignoring interclass correlations, as proved by Eq. 18.

4 Conclusions

The MCG approach for estimating threshold-exceeding probability maps was introduced and applied to a case study in spatial uncertainty assessment of clay layer thickness. Although the MCG approach needs to use four auto and cross transiogram models to deal with one threshold value, estimating a single transiogram model is sufficient to infer the others by making use of the properties of transition probabilities. The case study shows that by estimating the local conditional probability of a threshold class at each location from a number of simulated realizations, reasonable probability maps for different threshold values can be acquired. These probability maps reflect the spatial uncertainty of clay layer thickness (not exceeding some thresholds). They may be further hardened as binary maps based on different probability levels for representing certain “quality” areas under a certain

probability level. A comparison between MCG and conventional indicator kriging methods in estimating threshold-exceeding probabilities indicates that MCG provides a feasible method for spatial uncertainty assessment of continuous environmental variables with some advantages.

The study proves the following points: (i) when estimating threshold-exceeding probabilities, incorporation of cross-correlations of the two indicators (or classes) for a threshold value is valuable for generating reasonable results. Without incorporating cross-correlations, the estimated probabilities may be unreliable. (ii) For each approach, the threshold-exceeding probability map estimated through sequential simulation is more or less different from that estimated through interpolation. The former shows more reasonable patterns than the latter does. (iii) The probability map estimated through MCRF interpolation shows some undesirable uneven transitions, especially when samples are sparse and located unevenly. This may imply that the quadrant search is not perfect for interpolation to generate nice-looking maps, although it has long been a choice for reducing clustering in interpolation (Goovaerts 1997, p. 178). One way to remove the uneven transitions may be using a smoothing method to smooth the estimated conditional probability data.

In general, based on point (i), we think that the MCG approach is appropriate and has advantages for spatial uncertainty assessment of continuous spatial variables; and based on points (ii) and (iii), we recommend using sequential simulation rather than interpolation algorithms to estimate threshold-exceeding probability maps for spatial uncertainty assessment. This agrees with recent studies about using SIS for spatial uncertainty estimation. Although using sequential simulation to estimate probability maps will require more CPU time than using interpolation, it is not a major concern now for both SIS and MCSS because most CPUs of current personal computers have sufficient speeds to generate a large number of simulated realizations in a reasonable time using SIS and MCSS.

The MCG approach may be further extended by adding a time dimension to estimate the spatiotemporal state change of ecological variables. Many complex spatial ecosystems show threshold dynamics and abrupt changes in their states (Andersen et al. 2009; Contamin and Ellison 2009; Guttal and Jayaprakash 2009; Scheffer et al. 2009). Such state changes or transitions should be related to the spatial heterogeneity of the ecosystems. An important question in these systems concerns on determining whether such a state transition has happened and even more importantly whether such an abrupt change can happen in the near future. van Nes and Scheffer (2005) studied the implication of spatial heterogeneity for catastrophic regime shifts in ecosystems. Dakos et al. (2009) found that spatial

correlations might serve as a leading indicator of catastrophic shifts. Spatiotemporal geostatistics has been used to estimate the temporal change of some spatiotemporal variables such as ground water table (Christakos 2000). Markov chains were traditionally used for time series analysis of discrete states; it is in prospect that a spatiotemporal MCG might provide an effective statistical tool to detect or predict the temporal state transitions of a spatially heterogeneous ecosystem.

In this study, we did not compare the MCG approach with other approaches for threshold-exceeding probability estimation, such as disjunctive kriging (Armstrong and Matheron 1986), clipped Gaussian random fields (de Oliveira 2000) and generalized linear model (Gotway and Stroup 1997), although they each may have some advantages over indicator kriging. One reason is that our study was mainly focused on the sequential simulation strategy, but we did not find sequential simulation algorithms with software based on these methods. The second reason is that these methods are generally quite computationally demanding in case of large data sets and large maps (de Oliveira 2000; Lark and Ferguson 2004). In addition, disjunctive kriging and clipped Gaussian random fields also require an assumption of normality of data. Our data set in the case study (see Fig. 3) apparently does not meet this requirement.

Acknowledgement We would like to thank the anonymous reviewers for their constructive comments. Support from the Natural Science Foundation of China (Project No. 40971269) is greatly appreciated.

References

- Andersen T, Carstensen J, Hernandez-Garcia E, Duarte CM (2009) Ecological thresholds and regime shifts: approaches to identification. *Trends Ecol Evol* 24:49–57
- Arbia G, Lafratta G, Simeoni C (2007) Spatial sampling plans to monitor the 3-D spatial distribution of extremes in soil pollution surveys. *Comput Stat Data Anal* 51:4069–4082
- Armstrong M, Matheron G (1986) Disjunctive kriging revisited: part I. *Math Geol* 18:711–728
- Atkinson PM (1999) Geographical information science: geostatistics and uncertainty. *Prog Phys Geog* 23:134–142
- Brus DJ, de Gruijter JJ, Walvoort DJJ, de Vries F, Bronswijk JJB, Romkens PFAM, de Vries W (2002) Mapping the probability of exceeding critical thresholds for cadmium concentrations in soils in the Netherlands. *J Environ Qual* 31:1875–1884
- Chiles JP, Delfiner P (1999) *Geostatistics—modeling spatial uncertainty*. Wiley, New York, 695 pp
- Christakos G (2000) *Modern spatiotemporal geostatistics*. Oxford University Press, New York, 312 pp
- Contamin R, Ellison AM (2009) Indicators of regime shifts in ecological systems: what do we need to know and when do we need to know it? *Ecol Appl* 19:799–816
- Dakos V, van Nes EH, Donangelo R, Fort H, Scheffer M (2009) Spatial correlation as leading indicator of catastrophic shifts. *Theor Ecol*. doi: 10.1007/s12080-009-0060-6
- de Oliveira V (2000) Bayesian prediction of clipped Gaussian random fields. *Comput Stat Data Anal* 34:299–314
- Deutsch CV, Journel AG (1998) *GSLIB: Geostatistics Software Library and User's Guide*. Oxford University Press, New York, 370 pp
- Gaus I, Kinniburgh DG, Talbot JC, Webster R (2003) Geostatistical analysis of arsenic concentration in groundwater in Bangladesh using disjunctive kriging. *Environ Geol* 44:939–948
- Goovaerts P (1997) *Geostatistics for natural resources evaluation*. Oxford University Press, New York, 483 pp
- Goovaerts P (1999) Impact of the simulation algorithm, magnitude of ergodic fluctuations and number of realizations on the spaces of uncertainty of flow properties. *Stoch Environ Res Risk Assess* 13:161–182
- Goovaerts P (2001) Geostatistical modeling of uncertainty in soil science. *Geoderma* 103:2–26
- Goovaerts P, Webster R, Dubois P (1997) Assessing the risk of soil contamination in the Swiss Jura using indicator geostatistics. *Environ Ecol Stat* 4:31–48
- Gotway CA, Stroup WW (1997) A generalized linear model approach to spatial data analysis and prediction. *J Agric Bio Environ Stat* 2:157–178
- Guttal V, Jayaprakash C (2009) Spatial variance and spatial skewness: leading indicators of regime shifts in spatial ecological systems. *Theor Ecol* 11:450–460
- Jager HI, King AW, Schumaker NH, Ashwood TL, Jackson BL (2005) Spatial uncertainty analysis of population models. *Ecol Model* 185:13–27
- Journel AG (1983) Nonparametric estimation of spatial distributions. *Math Geol* 15:445–468
- Journel AG, Isaaks EH (1984) Conditional indicator simulation: application to a Saskatchewan uranium deposit. *Math Geol* 16:685–718
- Juang KW, Chen YS, Lee DY (2004) Using sequential indicator simulation to assess the uncertainty of delineating heavy-metal contaminated soils. *Environ Pollut* 127:229–238
- Lark RM, Ferguson RB (2004) Mapping risk of soil nutrient deficiency or excess by disjunctive and indicator kriging. *Geoderma* 118:39–53
- Li W (2007a) Markov chain random fields for estimation of categorical variables. *Math Geol* 39:321–335
- Li W (2007b) Transiograms for characterizing spatial variability of soil classes. *Soil Sci Soc Am J* 71:881–893
- Li W, Zhang C (2007) A random-path Markov chain algorithm for simulating categorical soil variables from random point samples. *Soil Sci Soc Am J* 71:656–668
- Li W, Zhang C (2009) Linear interpolation and joint model fitting of experimental transiograms for Markov chain simulation of categorical spatial variables. *Inter J Geogr Info Sci*. doi: 10.1080/13658810903127991
- Scheffer M, Bascompte J, Brock WA, Brovkin V, Carpenter SR, Dakos V, Held H, van Nes EH, Rietkerk M, Sugihara G (2009) Early-warning signals for critical transitions. *Nature* 461:53–59
- Schnabel U, Tietje O, Scholz RW (2004) Uncertainty assessment for management of soil contaminants with sparse data. *Environ Manag* 33:911–925
- Solow AR (1986) Mapping by simple indicator kriging. *Math Geol* 18:335–354
- Staff of the U.S. Bureau of Mines (1996) *Dictionary of mining, mineral, and related terms (CD-ROM)*. The U.S. Bureau of Mines. http://www.webref.org/geology/q/quadrant_search.htm. Accessed July 27, 2009
- Switzer P (1977) Estimation of spatial distributions from point sources with application to air pollution measurement. *Bull Int Stat Inst* 47:123–137

- van Groenigen JW, Stein A, Zuurbier R (1997) Optimization of environmental sampling using interactive GIS. *Soil Technol* 10:83–97
- van Meirvenne M, Goovaerts P (2001) Evaluating the probability of exceeding a site-specific soil cadmium contamination threshold. *Geoderma* 102:75–100
- van Nes EH, Scheffer M (2005) Implications of spatial heterogeneity for regime shifts in ecosystems. *Ecology* 86:1797–1807
- Wang G, Fang S, Shinkareva S, Gertner G, Anderson A (2002) Spatial uncertainty in prediction of the topographical factor for the revised universal soil loss equation (RUSLE). *Trans ASAE* 45:109–118
- Yang J, Huang Z-C, Chen T-B, Lei M, Zheng Y-M, Zheng G-D, Song B, Liu Y-Q, Zhang C (2008) Predicting the probability distribution of Pb-increased lands in sewage-irrigated region: a case study in Beijing, China. *Geoderma* 147:192–196
- Zhang C, Li W (2008a) Regional-scale modeling of the spatial distribution of surface and subsurface textural classes in alluvial soils using Markov chain geostatistics. *Soil Use Manag* 24:263–272
- Zhang C, Li W (2008b) A comparative study of nonlinear Markov chain models for conditional simulation of multinomial classes from regular samples. *Stoch Environ Res Risk Assess* 22:217–230
- Zhao Y, Shi X, Yu D, Wang H, Sun W (2005) Uncertainty assessment of spatial patterns of soil organic carbon density using sequential indicator simulation, a case study of Hebei province, China. *Chemosphere* 59:1527–1535